Role of multiband effects and electron-hole asymmetry in the superconductivity and normal state properties of $Ba(Fe_{1-x}Co_x)_2As_2$

Lei Fang[1], Huiqian Luo[1], Peng Cheng[1], Zhaosheng Wang[1], Ying Jia[1], Gang Mu[1], Bing Shen[1], I. I. Mazin[2], Lei Shan[1], Cong Ren[1] and Hai-Hu Wen[1⋆]

[1]*National Laboratory for Superconductivity, Institute of Physics and Beijing National Laboratory for Condensed Matter Physics, Chinese Academy of Sciences, P.O. Box 603, Beijing 100190, China and*

[2]*Code 6391, Naval Research Laboratory, Washington, DC 20375*

arXiv:0903.2418v3 [cond-mat.supr-con] 17 Oct 2009

We report a systematic investigation, together with a theoretical analysis, of the resistivity and Hall effect in single crystals of $Ba(Fe_{1-x}Co_x)_2As_2$, over a wide doping range. We find a surprisingly great disparity between the relaxation rates of the holes and the electrons, in excess of an order of magnitude in the low-doping, low-temperature regime. The ratio of the electron to hole mobilities diminishes with temperature and doping (away from the magnetically ordered state) and becomes more conventional. We also find a straightforward explanation of the large asymmetry (compared to cuprates) of the superconducting dome: in the underdoped regime the decisive factor is the competition between AF and superconductivity (SC), while in the overdoped regime the main role is played by degradation of the nesting that weakens the pairing interaction. Our results indicate that spin-fluctuations due to interband electron-hole scattering play a crucial role not only in the superconducting pairing, but also in the normal transport.

PACS numbers: 74.20.Rp, 74.25.Ha, 74.70.Dd

The discovery in the last year of new iron-based superconductors [1] provided a tempting analogy with high-T_c cuprates. Indeed, a simple comparison between phase diagrams reveals, particularly clearly for the $BaFe_2As_2$ family[2, 3, 4], a couple interesting similarities with the cuprates: first and foremost, the parent compound is an antiferromagnet (AFM), and spin fluctuations appear important for carrier pairing. Second, the superconductivity (SC) appears with either hole or electron doping, at a finite doping level, and forms a dome-shaped region in the phase diagram, as in cuprates.

A closer look, however, reveals equally striking differences: Indeed, unlike the cuprates, the parent compoundis in pnictides are metals that support quantum oscillations[5, 6], and the Coulomb correlations appear to be weak[7]. Second, unlike cuprates, superconductivity can be induced without doping, by external or chemical pressure[8]. Finally, the superconducting dome is very asymmetric[9, 10]. And, probably most importantly, electronic structure in cuprates is formed essentially by one band, while in the pnictiodes multiband effects are of primary importance.

The doping dependence of the evolution of the multiband electronic structure and its relationship to AFM, spin fluctuations, and SC is the key to the physics of the high-T_c ferropnictides. Systematic Hall coefficient and resistivity measurements are clearly well-suited to provide useful insight into these issues. In this Letter we select $BaFe_2As_2$ for a systematic study of the Hall effect and resistivity. Through quantitative analysis of the experimental data, combined with theoretical calculations, we establish a unified view of the doping induced evolution of SC and AFM, as well as the ramifications for the pairing mechanism.

The crystals were grown by self-flux method using FeAs as the flux; the details are described elswhere[11, 12]. The main advantage of the 122 system [2, 3, 4] is that it allows fabrication of large single crystals, and can be easily doped with holes[4, 13, 14] or with electrons[3, 11, 12, 15]. The crystal structure and chemical composition were checked by X-ray diffraction and energy dispersive X-ray microanalysis. The actual concentration of Co in the samples is found to be close to the nominal values. Measurements of the in-plane longitudinal (ρ_{xx}) and transverse (ρ_{xy}) resistances were carried out in a Physical Properties Measurement System (PPMS, Quantum Design) using the standard six probe method. All electronic calculations were performed using the Full Potential LAPW method as implemented in the WIEN2k package. The experimental crystal structure for $BaFe_2As_2$ was used for all calculations. Doping was taken into account through the rigid band approximation. The same setup was used as in Ref. [16].

Fig. 1(a) shows the resistivity for $Ba(Fe_{1-x}Co_x)_2As_2$ single crystals with doping levels ranging from the undoped parent phase to heavily overdoped compounds. With doping, the system evolves from AFM (with a resistivity anomaly) to superconductivity, and finally to a normal metal. The resistivity drops sharply at about 137 K in the parent phase, due to a drastic reduction of the scattering rate in the AF state that overcomes the reduction of the carrier concentration due to partial gapping of the FS [17, 18]. We have verified by first-principles calculations that in the fully spin polarized phase, that is, with the magnetic moment of at least 1.5 μ_B, the calculated Hall concentration is $n_h = n_e = 0.015$, as opposed to 0.15 in the nonmagnetic case, in quantitative agreement with the reduction of optical carrier concentration by a factor of 8 and the relaxation time [17] by a factor of 20. Interestingly, a rather small Co doping (2%) turns this sharp drop into an equally sharp (though smaller in magnitude) upturn (Fig. 1(a)). Assuming that the reduction in carrier concentration is comparable to that at $x = 0$, we observe that the reduction of the relaxation rate in the AFM state is at least 30% smaller in the 2%-doped samples than in the undoped ones. The evolution of the conductivity can be understood as follows: as-

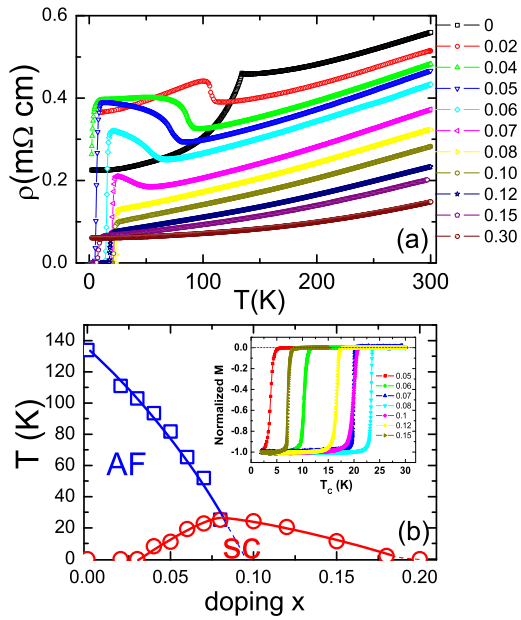

FIG. 1: (Color online) (a) Temperature dependence of the resistivity of $Ba(Fe_{1-x}Co_x)_2As_2$ single crystals. The maximal T_C occurs at about 25.2 K with a doping level of 8%, where the AF/structural transition cannot be explicitly resolved (but extrapolates to approximately the same temperature at $x \approx 8\%$). (b) The phase diagram derived from the resistivity and Hall effect measurements. We do not resolve the small splitting between the structural and AFM transitions. The inset shows the diamagnetic signal measured in superconducting samples.

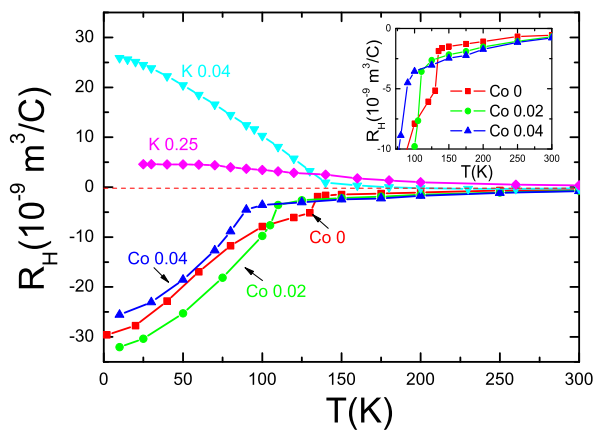

FIG. 2: (Color online) Temperature dependence of R_H for the parent phase, 4% and 25% K-doped $Ba_{1-x}K_xFe_2As_2$ crystals, 2% Co-doped and 4% Co-doped $Ba(Fe_{2-x}Co_x)_2As_2$ crystals. Note that a very small amount of K-doping leads to a sudden sign change of R_H in the AF state. The inset shows R_H near the AF transition for selected dopings.

suming that the main source of the transport relaxation is spin fluctuations, the freezing out of such fluctuations is more complete when the measured magnetic moments are larger. Fig. 1(b) shows the phase diagram of $Ba(Fe_{1-x}Co_x)_2As_2$ system derived from our data. The characteristic magnetic anomaly temperature, T_{AF}, is determined from resistivity and Hall coefficient measurements (both sets of data coincide within a few Kelvin). As mentioned, two points are of interest in regard to this phase diagram. One is the coexistence/competition between AFM and SC in the underdoped regime, the other is the asymmetric shape of the superconducting dome. The Hall measurements presented here provide a comprehensive explanation of both.

In Figs. 2 and 3 we present the Hall coefficient R_H throughout wide doping and temperature ranges (until recently, the Hall effect was measured only at limited doping levels [11]). The undoped samples provide the first major surprise. By definition, undoped samples are compensated, that is, $n_h = n_e = n_0$. The general formula for the Hall coefficient in the Boltzmann approximation reads [19]

$$R_H = \left(\sum \frac{\sigma_i^2}{n_i^H}\right) / \left(\sum \sigma_i\right)^2, \qquad (1)$$

where $\sigma_i = e^2(\frac{n}{m})_i\tau_i$ is the electrical conductivity in the ith band, $(\frac{n}{m}) = \frac{\omega_p^2}{4\pi e^2}$ is expressed in terms of the plasma frequency for the relevant crystallographic directions, and τ_i is the Boltzmann relaxation time. In the case of fully-compensated semimetals, like undoped pnictides, Eq. 1 reduces to

$$R_H = n_0^{-1}\frac{\sigma_h - \sigma_e}{\sigma_h + \sigma_e} = n_0^{-1}\frac{\mu_h - \mu_e}{\mu_h + \mu_e}, \qquad (2)$$

where $\mu = \sigma/n = \tau/m$ is the mobility. Contrary to a common misconception, the Hall coefficient in compensated or nearly compensated metals is hardly characteristic of the actual carrier concentrations, but is substantially reduced, unless one type of carrier has a much higher mobility than the other. It is therefore most puzzling that in the undoped samples $R_H = -30 \times 10^{-9}$ m^3/C, corresponding to 0.013 carrier per Fe. Since according to Eq.2, the carrier number n_0^{-1} gives the *upper* boundary for R_H, we are left to conclude that the actual n_0 is 0.01 or less, and that the transport is dominated by the electrons. This conclusion is supported by the concentration dependence of the low-T Hall coefficient, which reveals a smooth dependence with a sign change around 1.5% hole doping and a maximum of 32×10^{-9} m^3/C around 1.5% electron doping. This can again be reconciled within the same model, using the two-band version of Eq. 1:

$$R_H = \frac{n_h\mu_h^2 + n_e\mu_e^2}{(n_e\mu_e + n_h\mu_h)^2}. \qquad (3)$$

If $\mu_e \gg \mu_h$, then $R_H \approx 1/n_e$. However, at the hole doping with $x \sim n_0$ the electron pocket in the AF state disappears, and the Hall coefficient abruptly changes sign (cf. Fig. 2).

The normal state Hall data analysis also indicates that electrons dominate the transport. Just above the AFM transition,

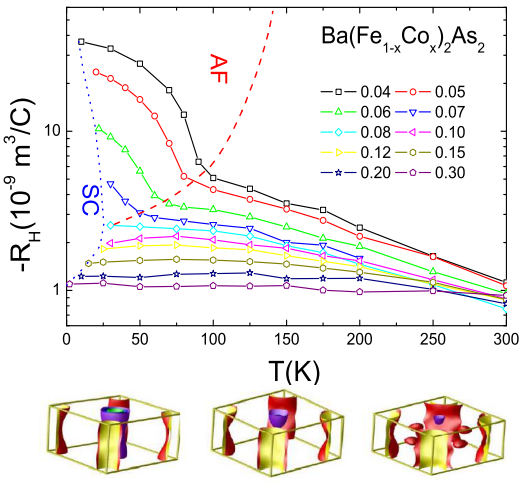

FIG. 3: (Color online) Upper panel: the temperature dependence of the Hall coefficient R_H at 9 T. The red dashed line at $x \lesssim 0.07$ follows T_{AF}, below which R_H rises sharply, indicating a dramatic change of the carrier concentration and scattering rate, as discussed in the text. The blue dotted line outlines the superconducting region. The lower panel (from left to right) represents the Fermi surfaces calculated for nonmagnetic $Ba(Fe_{1-x}Co_x)_2As_2$ for x =0, 0.2 and 0.3 (in the virtual crystal approximation).

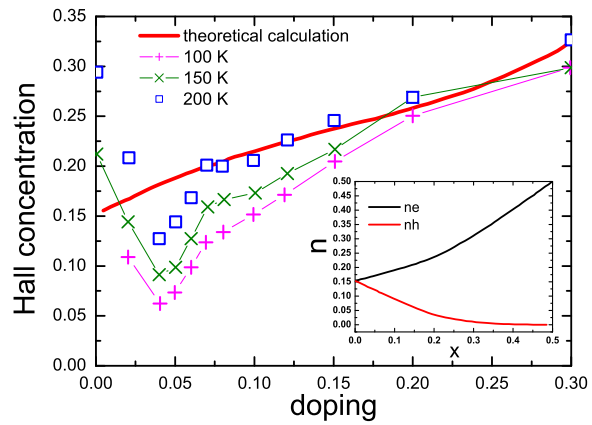

FIG. 4: (Color online) Electron concentration extracted from the Hall coefficient presented in the main text, as compared with the calculated Hall concentrations (solid line), assuming an x-dependent ratio of the electron and hole mobilities, $\mu_h/\mu_e = 1.3x$. The inset shows the calculated volumes of the hole and electron pockets as a function of electron doping, in the rigid band approximation.

R_H is reduced to a value corresponding to a carrier concentration of 0.21 e. Using the calculated nonmagnetic carrier concentration of 0.15 e, we can deduce from Eq. 2 that electron mobility at that temperature is about 6 times larger than the hole mobility. At higher temperatures, R_H continues to decrease with the temperature, reaching -0.56×10^{-9} m^3/C at $T = 300$ K (-0.56 e/Fe), corresponding now to $\mu_h \sim 0.6\mu_e$. To summarize this part, the high-temperature state of $BaFe_2As_2$ is consistent with the nonmagnetic band structure calculations, assuming that the hole mobility is smaller than the electron mobility at room temperature and becomes *much* smaller upon cooling (essentially negligible at $T \ll T_{AF}$).

Let us now turn to the electron doping. As explained above, the sharp increase of R_H is gradually less well expressed with doping, in accordance with the gradual suppression of the magnetism, but is still detectable in all samples where resistivity measurements indicate an AF transition (see Fig. 3). As in the undoped crystals, R_H continues to decrease upon heating above T_{AF}, albeit much slower than at low T. This indicates that for $x < 0.08$ even at room temperature magnetic fluctuations still affect the carrier concentration. At higher dopings this effect disappears, and the temperature dependence becomes rather moderate and essentially vanishes above $x \approx 0.2$, as the hole pockets practically close. The moderate T dependence at $0.08 < x < 0.2$ is readily understood in terms of a somewhat different T dependence for the hole and electron mobilities. Importantly, superconductivity vanishes at a doping level of 18–20%, where the temperature dependence of the Hall coefficient R_H disappears. This indicates that a multiband Fermi surface is a prerequisite for superconductivity. In the the lower panel of Fig. 3, we show the Fermi surfaces calculated at x =0, 0.2 and 0.3, in the rigid band model. Note that at $x = 0.2$ the hole pockets lose their 2D character (and 2D nesting) and practically disappear at $x = 0.3$.

It is also instructive to analyze the effective Hall concentration as a function of doping at high temperatures. As Fig. 4 shows, the dependence is non-monotonic, with three distinct regimes: one for $x \lesssim 0.04$, another for $0.04 \lesssim x \lesssim 0.08$, and the third for $x \gtrsim 0.08$. In the first regime the effective Hall concentration drops from a rather large number (twice larger than the calculated nonmagnetic n_0, as shown by the solid line) to a number even lower than n_0 at $x = 0.04$. In the two-band model that can have but one meaning: the ratio of the hole mobility to the electron mobility sharply decreases with doping. The fact that even at 200 K the minimal observed Hall concentration is 0.12, smaller than n_0, indicates that fluctuating spin density waves are still stealing some carriers even near room temperature. With further doping, however, this effect rapidly diminishes and at $x > 0.07$ the measured concentration (at 200 K) is consistent with the nominal concentration calculated from the band structure (see Fig.4). Comparung the upper line in the inset graph in Fig. 4. one can see that the electron-only concentration is close to the 200 K experimental data at $x > 0.07$, but slightly smaller than it even at $x > 0.2$. The difference is accunted for by small, but finite hole contribution.

As a result, the following picture emerges from our trans-

port measurements. In the formally stoichiometric, undoped compound at low temperatures, transport is dominated by electron pockets. Electron bands already have a higher mobility than the hole bands in the paramagnetic state, and the relaxation rate for the electrons (but not as much for the holes) decreases with cooling, and drops precipitously below T_{AF}. With doping, the gapping becomes less well expressed. At $x \sim 0.04$ there are already enough carriers to support superconductivity, while at $x \sim 0.08$ the gapping disappears and superconductivity enjoys the full density of states. In the overdoped regime, T_c is controlled by the strength of the available spin fluctuations. The quality of the quasi-nesting between the hole and the electron FSs is reduced with doping, and superconductivity disappears where the hole cylinders disappear at $x \sim 0.2$. In our present picture, we can naturally explain the asymmetric phase diagram [Fig.1(b)] because the suppression of T_c is governed by two different mechanisms in the underdoped and overdoped regimes.

The last corollary, very important for theories striving to explain the superconducting properties in pnictides, is that the relaxation rates of holes and electrons are very disparate. This may be the reason for the nonexponential behavior of such characteristics as penetration depth or the NMR relaxation rate. Also, this possibility needs to be taken into account when analyzing optical spectra (as turned out to be the case in MgB_2[20]). It is worth noting that in order to explain the temperature dependence of the upper critical fields in a 1111 compound within a two-band model, one needs at least an order of magnitude (possibly larger) disparity between the mobilities of the two bands, even though such an analysis cannot say which band is more mobile[21]. Finally, recent de Haas-van Alphen data also indicate a higher mobility of electrons [6].

In summary, we have demonstrated that the superconducting dome in pnictides has a very different origin from that of the cuprates. The underdoped side of the dome is defined by competition between AFM and superconductivity for the carrier density. In the overdoped regime superconductivity suffers from a suppression of the spin fluctuations and the loss of nesting. These two effects together lead to an asymmetric superconducting dome. Our second result is the surprisingly strong, and not readily understandable disparity of the scattering rates of the electron band and hole band. [22]

It is intriguing to ask if these finding are symmetric with respect to the doping sign. For instance in a hole-doped regime, would the mobility disparity survive, disappear, or change sign? This question will hopefully be answered by future experiments.

As a final note, recently similar measurements were reported by Rullier-Albenque $et\ al$[23]. Their results are very close to ours, and they also arrive at the conclusion that the only way to explain the Hall data at low temperatures and low doping is to assume a drastically suppressed hole mobility (compared to the electron one). They extend this assumption to all dopings and all $T < 150$ K (i.e., they assume the one-band model for the entire range), which we feel is not justified by the data. More importantly, they did not consider any effects of long-range AFM fluctuations on the carrier concentration. As a result, they were forced to introduce a thermally activated behavior for the electron density, which we believe is unphysical for this system, and requires not just renormalization of the LDA band structure, but abandoning it in a qualitative way.

This work was supported by the Natural Science Foundation of China(973 project No: 2006CB60100, 2006CB921107, 2006CB921802), and Chinese Academy of Sciences (Project ITSNEM). IIM was supported by the ONR.

⋆ hhwen@aphy.iphy.ac.cn

[1] Y. Kamihara *et al.*, J. Am. Chem. Soc. **130**, 3296 (2008).
[2] M. Rotter *et al.*, Angew. Chem. Int. Ed. **47**, 7949 (2008).
[3] A. S. Sefat *et al.*, Phys. Rev. Lett. **101**, 117004 (2008).
[4] M. Rotter *et al.*, Phys. Rev. Lett. **101**, 107006 (2008).
[5] S. E. Sebastian *et al.*, J. Phys.: Condens. Matter **20**, 422203 (2008).
[6] A. I. Coldea *et al.*, Phys. Rev. Lett. **101**, 216402 (2008); J. G. Analytis *et al.*, Phys. Rev. Lett. **103**, 076401 (2009).
[7] W. L. Yang *et al.*, Phys. Rev. **B 80**, 014508(2009); see also Z. Tesanovic, Phys. **2**, 69(2009).
[8] P. A. Alireza *et al.*, J. Phys.: Condens. Matter **21**, 012208 (2009).
[9] J. Zhao *et al.*, Nature Materials **7**, 953 (2008).
[10] A. J. Dew *et al.*, Nature Materials **8**, 310(2009).
[11] J.-H. Chu *et al.*, Phys. Rev. B **79**, 0145064 (2009).
[12] N. Ni *et al.*, Phys. Rev. B **78**, 214515 (2008).
[13] N. Ni *et al.*, Phys. Rev. B **78**, 014507 (2008).
[14] H.-Q. Luo *et al.*, Supercond. Sci. Technol. **21**, 125014 (2008).
[15] G. Cao *et al.*, Phys. Rev. B **79**, 054521 (2009).
[16] I. I. Mazin, *et al.*, Phys. Rev. **B78**, 085104 (2008).
[17] W. Z. Hu *et al.*, Phys. Rev. Lett. **101**, 257005 (2008).
[18] M. Tropeano *et al.*, Supcond. Sci. Tech. **22**, 034004 (2009).
[19] N. W. Ashcroft, and N. D. Mermin, Solid State Physics, Thompson Learning, Inc. 1976.
[20] A. B. Kuz'menko *et al.*, Solid State Comm. **121**, 479 (2002).
[21] J. Jaroszynski *et al.*, Phys. Rev. B. **78**, 174523 (2008).
[22] As a word of caution, our analysis is based on the two-band Fermi liquid theory. Strong non-Fermi-liquid effects, such as spin-charge separation, or strong angular anisotropy of the relaxation rate, may provide alternative interpretation of our Hall data. We do not see, however, any physical reasons for either of these effects here.
[23] F. Rullier-Albenque *et al.*, Phys. Rev. Lett. **103**, 057001 (2009).